Viscoelastic Effects in Avalanche Dynamics: A Key to Earthquake Statistics

E. A. Jagla
Centro Atómico Bariloche and Instituto Balseiro, Comisión Nacional de Energía Atómica, (8400) Bariloche, Argentina

François P. Landes and Alberto Rosso
Laboratoire de Physique Théorique et Modèles Statistiques (UMR CNRS 8626), Université Paris-Sud, Orsay, France

(Received 4 November 2013; revised manuscript received 11 January 2014; published 30 April 2014)

In many complex systems a continuous input of energy over time can be suddenly relaxed in the form of avalanches. Conventional avalanche models disregard the possibility of internal dynamical effects in the interavalanche periods, and thus miss basic features observed in some real systems. We address this issue by studying a model with viscoelastic relaxation, showing how coherent oscillations of the stress field can emerge spontaneously. Remarkably, these oscillations generate avalanche patterns that are similar to those observed in seismic phenomena.

DOI: 10.1103/PhysRevLett.112.174301 PACS numbers: 46.65.+g, 46.55.+d, 83.60.Df, 91.30.−f

The driven dynamics of heterogeneous systems often proceeds by random jumps called *avalanches*, which display scale-free statistics. This critical out-of-equilibrium behavior emerges from the competition between internal elastic interactions and interactions with heterogeneities, and is understood in the framework of the depinning transition [1,2]. Remarkably, one can often disregard the precise details of the microscopic dynamics when considering the large scale behavior. As a result, various phenomena such as Barkhausen noise in ferromagnets [3–5], crack propagation in brittle materials [6–8] or wetting fronts moving on rough substrates [9–11] may display similar avalanche statistics.

In this description of avalanches a trivial dynamics in the interavalanche periods is usually assumed [1,12]. However, the inclusion of viscoelastic effects with their own characteristic time scales brings about novel dynamical features. The existence of this kind of relaxation may have drastic consequences on the macroscopic behavior of the system, as in the context of friction where it generates the time increase of static friction during the contact between two surfaces at rest [13,14]. Here we show how these relaxation processes generically induce a novel avalanche dynamics characterized by new critical exponents and bursts of aftershocks strongly correlated in time and space. Because of its simplicity, the model allows for analytic treatment in the mean field, and for extensive numerical simulations in finite dimensions. Our main observations are twofold. First, in the mean field the time scale of viscoelastic relaxation is associated with a dynamical instability, which we prove to be responsible for periodic oscillations of the stress in the entire system. This instability, named *avalanche oscillator*, was observed in numerical simulations and experiments of compression of Nickel microcrystals [15]. Note that viscoelastic interactions are also at the root of the hysteretic depinning emerging in mean field periodic systems like vortex lattice or charge density waves [16,17]. Second, in two dimensions the global oscillations found in the mean field remain coherent only on small regions. In each region the oscillations of the local stress have roughly the same amplitude and period but different phases, so that at a given time the stress map has a terraced structure.

We claim that the relaxation processes studied in our model are essential to capture the basic features of seismic dynamics. In particular, the viscoelastic time scale is the one involved in the aftershock phenomenon [18–20]. Moreover the oscillations of the stress field explain the quasiperiodic time recurrence of earthquakes that emerges from the data analysis of the seismic activity in some geographical areas [21,22]. Finally we show that in two dimensions, viscoelastic relaxation produces an increase in the exponent of the avalanche size distribution compatible with the Gutenberg-Richter law, and the aftershock spatial correlations obtained have strong similarities with the so-called *migration effect* observed in real earthquakes [23].

The models.—Our model with relaxation is constructed upon the paradigmatic model of avalanche dynamics, describing the depinning of a d-dimensional elastic interface moving inside a $(d+1)$-dimensional space [1]. In this model, the interface consists of a collection of blocks [see Fig. 1(a)] obeying the equation of motion,

$$\eta \partial_t h_i = k_0(w - h_i) + f_i^{\mathrm{dis}}(h_i) + k_1 \Delta h_i \qquad (1)$$

where (i, h_i) is the $(d+1)$-dimensional coordinate of the block and η is the viscosity of the medium. Each block feels elastic interactions via the (discrete) Laplacian term $k_1(\Delta h)_i = k_1 \sum_{\langle ij \rangle}(h_j - h_i)$ (summation is restricted to nearest neighbors of i), disorder via $f_i^{\mathrm{dis}}(h_i)$ and is driven towards the position $w = V_0 t$ via springs of elasticity k_0.

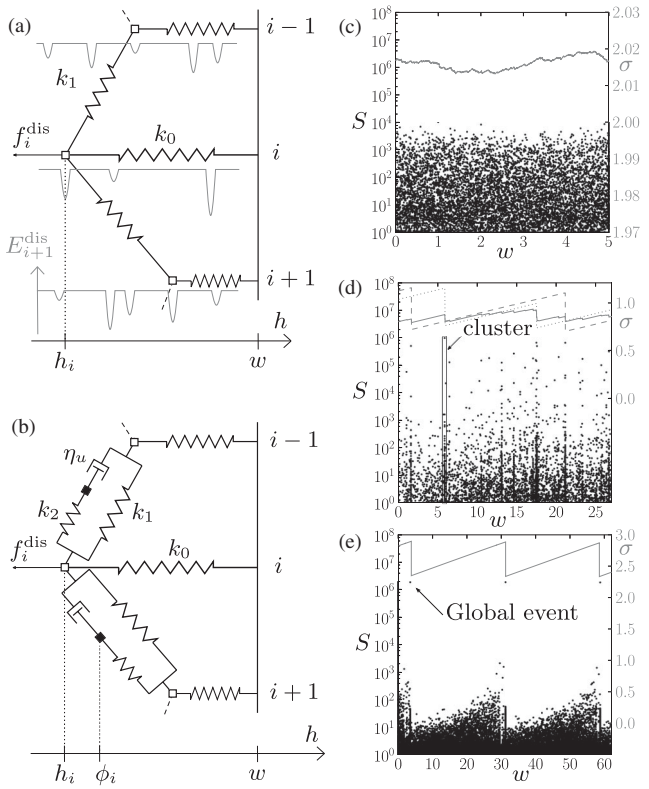

FIG. 1. Sketch of the models for $d = 1$. (a) Conventional depinning model: disorder and elastic interactions acting on the blocks, located in h_i, h_{i+1}, etc. The disordered force derives from the pinning potential (gray): $f_i^{\mathrm{dis}} = -\partial E_i^{\mathrm{dis}}(h_i)/\partial h_i$. (b) Depinning with relaxation: we introduce dashpots with relaxation constant η_u and springs of stiffness k_2. Right: numerical results showing sequences of avalanches sizes S (dots) and stress (continuous lines) as a function of drive w for: the elastic depinning model in $d = 2$ (c), the depinning with relaxation in $d = 2$ (d) (dashed and dotted lines correspond to local stress in two distant regions), and in the mean field (e).

The force per unit area applied by the drive, namely, the stress is given by $\sigma = k_0(w - \bar{h})$, where $\bar{h} = (1/N)\sum h_i$ is the mean value of interface height ($N = L^d$). The slow increase of w over time induces an augmentation of the pulling force on each block. As a response, blocks typically slightly adjust their positions, but sometimes a block reaches a mechanically unstable state and moves far away from its position to a new local energy minimum. This can in turn destabilize neighboring blocks, thus triggering an avalanche event that we characterize by its size $S = N(\bar{h}_{\mathrm{after}} - \bar{h}_{\mathrm{before}})$, which is simply the volume swept by the interface during the event. In Fig. 1(c) we show the sizes S of a sequence of avalanches obtained by driving w quasistatically ($V_0 = 0^+$). The sequence displays an almost Poissonian behavior, in the sense that both the sizes and the time occurrences of the events are almost uncorrelated variables. Moreover the stress is constant in time, with fluctuations due to finite system size.

Our modified model consists in replacing springs k_1 by viscoelastic elements, built using springs and dashpots as depicted in Fig. 1(b). Dynamical equations become

$$\eta \partial_t h_i = k_0(w - h_i) + f_i^{\mathrm{dis}}(h_i) + k_1 \Delta h_i + k_2(\Delta h_i - u_i),$$
$$\eta_u \partial_t u_i = k_2(\Delta h_i - u_i), \tag{2}$$

where the auxiliary variables u_i depend on the elongation of the neighboring dashpots: in one dimension this variable reads $u_i = (\phi_i - h_i) + (h_{i-1} - \phi_{i-1})$ (see the Supplemental Material [24]). The relaxation constant η_u sets a new characteristic time $\tau_u = \eta_u/k_2$, to be compared with the two scales: (i) $\tau_D = \bar{z}/V_0$ which accounts for the slow increase of the external drive w (where $\bar{z}$ is the typical microscopic disorder length scale, defined later), (ii) $\tau = \eta/\max[k_0, k_1, k_2]$, which is the response time of the h variables. Essentially, "main" avalanches are triggered by the drive through k_0, whereas relaxation (via k_2, η_u) triggers additional events on a time scale of order τ_u: the aftershocks.

In our analysis, we assume that the three scales are well separated, namely, $\tau \ll \tau_u \ll \tau_D$ (i.e., $\eta \ll \eta_u$). Hence, on the time scale τ the u_i's are constant in time and the dynamics is exactly the same as for the depinning model with elastic constant $k_1 + k_2$. However, after an avalanche, and in a time scale $\tau_u \gg \tau$, h_i's are pinned (due to the narrow wells approximation, see below) and u_i's relax exponentially,

$$u_i(t) = \Delta h_i + (u_i(t_0) - \Delta h_i)e^{-(t-t_0)k_2/\eta_u}, \quad \forall\ i, \tag{3}$$

where t_0 is the time at which the last avalanche occurred. The effect of relaxation is to suppress the term $k_2(\Delta h_i - u_i)$ in Eq. (2), so that some blocks may become unstable. This triggers secondary avalanches in the system, identified with aftershocks in the seismic context. Aftershocks occur without any additional driving: the ensemble of events that occur at a given w will be called a *cluster* [Fig. 1(d)]. When $u_i = (\Delta h)_i\ \forall\ i$, the system is fully relaxed and new instabilities can only be triggered by an increase of w. Note that the fully relaxed configuration corresponds to a stable configuration of the depinning model with the same disorder realization and elastic constants k_0, k_1.

We mostly have in mind the $d = 2$ case, which is the one realized in the seismic context. We consider local elastic interactions for implementation convenience. Realistic long range interactions within the faults (induced by the three-dimensional nature of the plates) may have effects on the results we present, that are difficult to assess without a full numerical simulation. This remains as a prospect for future work.

The narrow wells approximation.—To efficiently study Eqs. (1,2), we adopt the so-called *narrow wells* approximation. In this scheme, disorder is modeled as a collection of narrow pinning wells representing impurities [see

Fig. 1(a)], with spacings z, distributed as $g(z)$ and with average $\bar{z} = \int_0^\infty z g(z) dz$. The maximum value of the pinning force at each well is denoted f^{th} (see the Supplemental Material [24]). Thanks to this choice, the system state can be reduced to a variable δ_i. In the depinning model

$$\delta_i \equiv f_i^{\text{th}} - k_0(w - h_i) - k_1 \Delta h_i. \quad (4)$$

As soon as $\delta_i \leq 0$, this site becomes unstable: an avalanche is triggered. The avalanche evolution translates into simple rules for δ_i's. When $\delta_i > 0, \forall\ i$, all blocks are stable and the avalanche is exhausted. Driving then follows until a new event is triggered.

In our model, δ_i's read

$$\delta_i = f_i^{\text{th}} - k_0(w - h_i) - k_1 \Delta h_i - k_2(\Delta h_i - u_i). \quad (5)$$

The dynamics proceeds as before, with u_i's kept constant during avalanches. When the avalanche is exhausted, a slow relaxation of u_i takes place [Eq. (2)]. This evolution can decrease δ_i's and thus trigger aftershocks.

Mean-field analysis.—We analyze the mean field, fully connected model, which corresponds to replacing Δh_i with $\bar{h} - h_i$ in Eqs. (4), (5). In this case, all sites are equivalent and the δ_i's are independent and identically distributed variables, characterized by the probability distribution $P_w(\delta)$ which in general depends on the initial condition $P_0(\delta)$ and on w. In the Supplemental Material [24], we obtain the evolution of $P_w(\delta)$ under an infinitesimal increase in w for both models, for $f_i^{\text{th}} = \text{const.}$

For the elastic depinning model, we show that this evolution has a fixed point reached within a finite increase in w, at which $P_w(\delta)$ is given by the function

$$Q(\delta, k_1) = \frac{1 - G(\delta/(k_0 + k_1))}{\bar{z}(k_0 + k_1)}, \quad (6)$$

where $G(z) \equiv \int_0^z dz' g(z')$. This indicates that the large time dynamics is stationary, and that the applied stress in the system is constant in time: $\sigma(k_1) \equiv f^{\text{th}} - \bar{\delta}(k_1)$. Further analysis shows that as long as $P_w(0) < (\bar{z}k_1)^{-1}$ the system displays avalanches bounded by a system-size independent cutoff: $S_{\max} = [1 - P_w(0)\bar{z}k_1]^{-2}$. For example, at the fixed point (6) we have $P_w(0) = Q(0, k_1) = 1/\bar{z}(k_0 + k_1)$, so that $S_{\max} = (1 + k_1/k_0)^2$. However if $P_w(0) \geq (\bar{z}k_1)^{-1}$ the system becomes unstable, with a global event, that involves a finite fraction of the system.

For the model with relaxation, the evolution of $P_w(\delta)$ is nonstationary and displays oscillations in time. Under a small increase in w, two dynamical regimes are observed. On short times ($t \simeq \tau$), sites that become unstable move following the rules of a rigid elastic interface, with stiffness $k_1 + k_2$. On longer times ($t \simeq \tau_u$), during relaxation, the interface becomes more flexible (stiffness k_1), thus evolving towards the fixed point $Q(\delta, k_1)$ (stages 1 and 2 in Fig. 2). However, when $P_w(0)$ becomes larger than $1/\bar{z}(k_1 + k_2)$, the rigid interface is unstable so that a single global avalanche drives $P_w(\delta)$ to the rigid fixed point $Q(\delta, k_1 + k_2)$ (stage 3 in Fig. 2). Finally, this state is altered by relaxation and a new cycle starts (stage 4).

Note that cyclic behavior is independent of the details of the mean field model: e.g., Fig. 1(e) corresponds to the case of randomly distributed thresholds f_i^{th}. The avalanche dynamics is different and displays aftershocks, but global events and stress oscillations are also present.

A similar viscoelastic model (with $k_1 = 0$, periodic disorder and under constant force F) was originally introduced [16,17,25] to model the hysteretic depinning observed in vortex lattices and charge density waves. In the fully connected approximation a self-consistent calculation pointed out that the average velocity is multivalued, yielding hysteretic behavior in a wide range of external stress. This hysteresis echoes with the oscillations in Fig. 2. Yet, in two dimensions, we see that constant velocity driving produces stress distributions that are not uniform, nor constant, and we get qualitative new results that were not obtained in the constant applied force case studied in Refs. [16,17,25].

Two-dimensional results.—For $d = 2$ we must rely on the numerical implementation of Eqs. (5), (3) via an efficient method originally developed in Ref. [26] (see the Supplemental Material [24]). In Fig. 1(d), we see a clear distribution of events in clusters of main shocks and aftershocks, as in actual seismicity (where, indeed, any

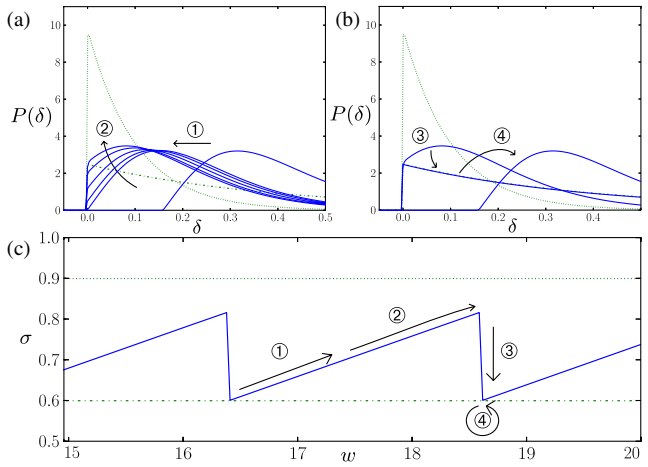

FIG. 2 (color online). Evolution of $P(\delta)$ [(a) and (b), solid line] and of the stress $\sigma = k_0(w - \bar{h})$ (c) computed from direct integration of the evolution equations. (1) driving without any avalanche, linearly increasing stress; (2) driving with elastic-depinning avalanches, slower stress increase. (3) global event: $P(\delta)$ collapses to the depinning fixed point $Q(\delta, k_1 + k_2)$ (lower dashed curve) and the stress drops to $\sigma(k_1 + k_2)$ (lower dashed line). (4) relaxation closes the cycle back to stage (1) without altering average stress.

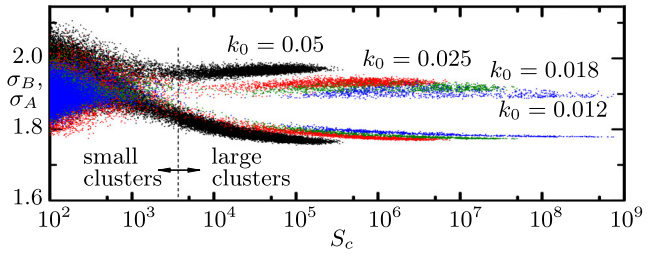

FIG. 3 (color online). The local stress restricted to the cluster area, just before (up, σ_B) and just after (bottom, σ_A) it takes place, as a function of the cluster size S_C. Thus, in, e.g., a compression experiment, one expects the average local variation of stress to vanish (with undefined values of $\sigma_{B,A}$) for small avalanches, and to saturate to a constant (nonzero) value (with well-defined values for $\sigma_{B,A}$) for large avalanches.

single cluster spans a finite w interval, due to the incomplete separation of time scales). The periodicity of the mean field [Fig. 1(e)] has now disappeared.

Nevertheless, a careful analysis of the $d = 2$ model shows an interesting reminiscence of the mean field behavior. In Fig. 3 we compute for each cluster the local stress restricted to the cluster area, just before (σ_B) and just after (σ_A) it takes place (the same analysis for events instead of clusters yields the same results). Small clusters show broad distributions of σ_B and σ_A, similar to what would be observed for the depinning case. However, for large clusters both distributions become very narrow: σ_B sets to a value that we denote $\sigma_{\max}$, and σ_A sets to $\sigma_{\min}$. This is the fingerprint of the mean field behavior, suggesting a large scale description of the $d = 2$ interface as a terraced structure. Indeed, we observe (Fig. 4) that different parts of the system have different values of the stress, which range from $\sigma_{\min}$ to $\sigma_{\max}$. In analogy with the mean field, when the stress of a region reaches a value $\sim\sigma_{\max}$, it gets destabilized and the whole region collapses to $\sigma_{\min}$. In fact the evolution of the local stress associated with a small patch of the interface is nonstationary, and shows an almost periodic oscillation between $\sigma_{\min}$ and $\sigma_{\max}$ [Fig. 1(d), dashed and dotted lines]. However this oscillation is not synchronized among different patches, so the system does not display a global oscillation. It is remarkable that the width of the distribution of the local stress ($\sim\sigma_{\max} - \sigma_{\min}$) remains finite when $k_0 \to 0$, while in the depinning model [27], it vanishes as $k_0^{1-\zeta/2}$ for very small k_0 (ζ is the roughness exponent of the interface which is found to be smaller than 2). Moreover our model supports the idea that seismic activity in some geographical regions displays quasiperiodicity (the so-called *seismic cycle* [19]). This periodicity was recently studied in the context of microcrystals deformation [15], where it was named *avalanche oscillator*. Similar kinds of oscillations were also observed in models with relaxation [27], granular materials [28], and molecular dynamics of viscoelastic disordered systems [29].

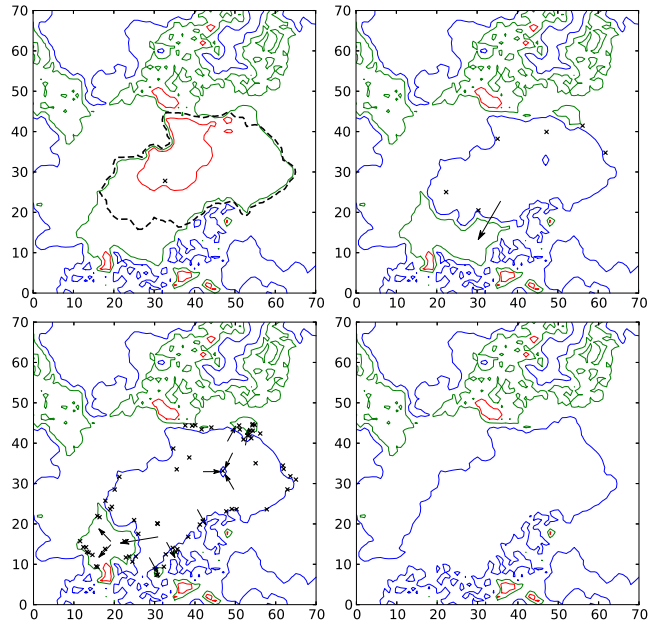

FIG. 4 (color online). Stress map in $d = 2$. Colors indicate stress levels, from high (red) to low (blue). Upper left: stress map just before a large event, with the unstable region highlighted by a dashed line. From left to right and top to bottom: expansion of the affected area is seen to mainly spread (black arrows) around the initial main shock and the subsequent aftershocks (small crosses). Affected regions have low chance to witness new large events, due to the low value of the local stress.

A second important feature is the spatial distribution of aftershocks in a given cluster (see Fig. 4). After a main shock, many aftershocks follow, extending the slip area. The small ones (not indicated) are rather uniformly distributed inside the slip region; while the epicenters of the large ones typically occur at the border, extending the slip region. Field observations report this effect as "aftershock migration" [23].

As a third point, we discuss the size distribution of the avalanches in 2D, presented in Fig. 2 of the Supplemental Material [24]. We find a consistent power law decay in all of the ranges that we have been able to explore (at least in a size range of 10^7) with an anomalous exponent $\kappa \simeq 1.7$–1.8. This is quite remarkable, given that in all conventional avalanche models like depinning or directed percolation, this exponent is always smaller than 1.5, which corresponds to the mean field limit [30,31]. In particular in the 2D depinning case one measures $\kappa \simeq 1.27$ [32]. Our result can be compared with the value for actual earthquakes where κ values in the range $\simeq 1.7 \pm 0.2$ are reported [33]. However, since we do not consider realistic long range elastic interactions, this coincidence has to be taken with caution. We also note that a justification for the value of the Gutenberg-Richter exponent has been given recently using a forest fire model analogy [34]. It is worth mentioning that arguments in Ref. [34] build upon a model that has a

terraced structure of the interface compatible with the one we find here.

Conclusions.—Internal relaxation plays a crucial role in the dynamics of sliding objects, and becomes particularly important at large scales, relevant to seismic phenomena. The dynamics of our model shows a strong tendency to become nonstationary. This tendency is manifest in the mean field, where sliding proceeds as a sequence of global and periodic stick slips. In $d = 2$, we provide numerical evidence that periodic stick slips occur locally, without global synchronization across the system. There, our predictions mainly deal with spatial properties of events, thus demanding high spatial resolution in experiments.

We thank Shamik Gupta and Mikhail B. Zvonarev for useful discussions. We acknowledge support from the France-Argentina MINCYT-ECOS A12E05. E. A. J. is financially supported by CONICET (Argentina). Partial support from Grant No. PICT-2012-3032 (ANPCyT, Argentina) is also acknowledged.

[1] D. S. Fisher, Phys. Rep. **301**, 113 (1998).
[2] M. Kardar, Phys. Rep. **301**, 85 (1998).
[3] B. Alessandro, C. Beatrice, G. Bertotti, and A. Montorsi, J. Appl. Phys. **68**, 2901 (1990).
[4] S. Zapperi, P. Cizeau, G. Durin, and H. E. Stanley, Phys. Rev. B **58**, 6353 (1998).
[5] G. Durin and S. Zapperi, J. Stat. Mech. (2006) P01002.
[6] M. J. Alava, P. K. V. V. Nukala, and S. Zapperi, Adv. Phys. **55**, 349 (2006).
[7] D. Bonamy, S. Santucci, and L. Ponson, Phys. Rev. Lett. **101**, 045501 (2008).
[8] D. Bonamy and E. Bouchaud, Phys. Rep. **498**, 1 (2011).
[9] A. Rosso and W. Krauth, Phys. Rev. E **65**, 025101 (2002).
[10] S. Moulinet, A. Rosso, W. Krauth, and E. Rolley, Phys. Rev. E **69**, 035103 (2004).
[11] P. Le Doussal, K. J. Wiese, S. Moulinet, and E. Rolley, Europhys. Lett. **87**, 56 001 (2009).
[12] J. P. Sethna, K. A. Dahmen, and C. R. Myers, Nature (London) **410**, 242 (2001).
[13] J. H. Dieterich, J. Geophys. Res. **77**, 3690 (1972).
[14] C. Marone, Nature (London) **391**, 69 (1998).
[15] S. Papanikolaou, D. M. Dimiduk, W. Choi, J. P. Sethna, M. D. Uchic, C. F. Woodward, and S. Zapperi, Nature (London) **490**, 517 (2012).
[16] M. C. Marchetti, A. A. Middleton, and T. Prellberg, Phys. Rev. Lett. **85**, 1104 (2000).
[17] M. C. Marchetti, arXiv:cond-mat/0503660.
[18] J. H. Dieterich, Pure Appl. Geophys. **116**, 790 (1978).
[19] C. H. Scholz, *The Mechanics of Earthquakes and Faulting* (Cambridge University Press, Cambridge, England, 2002).
[20] Y. Ben-Zion, Rev. Geophys. **46**, RG4006 (2008).
[21] S. Barbot, N. Lapusta, and J.-P. Avouac, Science **336**, 707 (2012).
[22] Y. Ben-Zion, J. Geophys. Res. **108**, 2307 (2003).
[23] Z. Peng and P. Zhao, Nat. Geosci. **2**, 877 (2009).
[24] See Supplemental Material at http://link.aps.org/supplemental/10.1103/PhysRevLett.112.174301 for details. In Sec. 1, the equations of motion for the viscoelastic model are derived from Newton's equations, and the narrow wells approximation is discussed. In Sec. 2, we give additional insight for the analytics of the mean field. In Sec. 3, we provide the pseudocode for the integration of the Fokker-Planck equations. In Sec. 4, we describe the idea of the Monte Carlo simulation used in 2D. In Sec. 5, details of the parameters used in all simulations are given.
[25] P. Le Doussal, M. C. Marchetti, and K. J. Wiese, Phys. Rev. B **78**, 224201 (2008).
[26] P. Grassberger, Phys. Rev. E **49**, 2436 (1994).
[27] L. E. Aragón, E. A. Jagla, and A. Rosso, Phys. Rev. E **85**, 046112 (2012).
[28] K. A. Dahmen, Y. Ben-Zion, and J. T. Uhl, Nat. Phys. **7**, 554 (2011).
[29] K. M. Salerno and M. O. Robbins, arXiv:1309.1872.
[30] P. Le Doussal and K. J. Wiese, Phys. Rev. E **79**, 051105 (2009).
[31] A. Dobrinevski, P. Le Doussal, and K. J. Wiese, Phys. Rev. E **85**, 031105 (2012).
[32] A. Rosso, P. Le Doussal, and K. J. Wiese, Phys. Rev. B **80**, 144204 (2009).
[33] Note that historically the magnitude of an earthquake is defined as $M = (2/3)\log_{10} S$. The Gutenberg-Richter law states that $N(M) \sim 10^{-bM}$, with reported values of b in the range 1 ± 0.25, so that from the definition $N(S) \sim S^{-\kappa}$, we obtain approximately $\kappa = 1 + 2b/3 \simeq 1.7 \pm 0.2$.
[34] E. A. Jagla, Phys. Rev. Lett. **111**, 238501 (2013).